7-15-2021

Ductility and Overstrength of Shape-Memory-Alloy Reinforced-Concrete Shear Walls

Emad A. Abraik
The University of Western Ontario

Maged A. Youssef
Western University, youssef@uwo.ca

Citation of this paper:
Abraik E., **Youssef M.A.**, 2021, "Ductility and Overstrength of Shape-Memory-Alloy Reinforced-Concrete Shear Walls", Engineering Structures, 239: 112236, https://doi.org/10.1016/j.engstruct.2021.112236.

Ductility and Overstrength of Shape-Memory-Alloy Reinforced-Concrete Shear Walls

Emad Abraik, Maged A. Youssef

Western University, Civil and Environmental Engineering, London, ON N6A 5B9, Canada

Abstract: The unique properties of superelastic shape-memory-alloy (SMA) bars have motivated researchers to investigate their use as reinforcing bars for concrete elements. They were found to decrease seismic residual deformations, while increasing seismic inelastic deformations. This characteristic deformation behaviour requires an assessment of the seismic design parameters of SMA reinforced concrete walls. This paper addresses this requirement by evaluating their ductility and overstrength factors. A total of 972 walls were analyzed under a quasi-static lateral load. Suitable values for the overstrength and ductility factors were estimated for two proposed locations of SMA bars. FEMA P695 was then utilized to evaluate the seismic safety margin for case study buildings, which were designed based on the estimated seismic design parameters.

Keywords: Shear wall, superelastic shape memory alloy, cyclic behaviour, response modification factor, overstrength, ductility.

Corresponding author: Maged A. Youssef, Email: youssef@uwo.ca, Tel.: 1-519-661-2111 Ext. 88661.

1. Introduction

During the past decade, researchers have shown that using superelastic shape memory alloy (SMA) bars in concrete elements results in sustainable structures. Following strong seismic events, such structures can be easily repaired, leading to significant cost savings, as compared to conventional structures [1]. With the current demand for self-centering structures, the use of SMA bars in reinforced concrete (RC) structures is expected to be a reality.

Extensive experimental and analytical studies have been conducted to explore the use of SMA bars in concrete structures. Youssef et al. [2] experimentally examined the cyclic performance of a beam-column joint that utilized SMA bars in the plastic hinge region. The SMA RC beam-column joint recovered most of its post-yield deformations. The seismic performance of full-scale frames reinforced with SMA bars was numerically investigated by Alam et al. [3] and Youssef and Elfeki [1]. Test results showed that SMA RC frames could recover their inelastic deformations even after strong seismic events. Abdulridha [4] conducted a large-scale cyclic test on an intermediate-height wall, which utilized SMA bars in the plastic hinge region. Significant deformation recovery was observed. Tazarv and Saiidi [5] experimentally assessed the seismic performance of a full-scale SMA RC bridge column. The results showed that the use of SMA bars reduced the residual drifts and limited the amount of damage in the plastic hinge zone.

Effendy et al. [6] experimentally evaluated the use of external superelastic SMA bars to improve the seismic performance of existing squat walls. Ghassemieh et al. [7] numerically investigated the seismic performance of RC walls equipped with SMA bars and concluded that the use of SMA bars resulted in reasonable improvement in seismic response in terms of reduced residual strains. Using numerical analyses, Abraik and Youssef [8, 9] highlighted the significant effect of the number and locations of SMA bars on the residual displacements of RC walls. They also numerically proved that

SMA bars can reduce damage to coupling beams and residual displacements of RC coupled walls [10,11]. Abraik and Youssef [12] numerically investigated the seismic performance and vulnerability of SMA RC walls and confirmed their superior seismic performance, as compared to steel RC walls. The seismic performance of SMA dual systems, which consist of SMA RC walls and SMA RC frames, was numerically investigated by Abraik and Youssef [13]. SMA RC dual systems were found to have superior seismic performance over steel RC dual systems. Kian and Cruz-Noguez [14] experimentally showed that SMA bars could reduce seismic residual drifts while offering acceptable levels of energy dissipation and ductility.

Previous experimental and numerical studies did not examine the seismic design characteristics of SMA RC walls. This paper addresses this shortcoming and, thus, paves the way for their future use. The examined seismic design characteristics are the ductility μ, the response modification factor R, and the over-strength factor Ω.

2. Displacement Ductility and Overstrength

Figure 1 shows the relationship between the seismic base shear and the top displacement of a typical RC building. The relationship can be simplified to a bilinear curve with a peak lateral strength Vy, yield displacement Δy (at which the lateral stiffness of the building is significantly reduced), and maximum displacement Δmax. Yielding is assumed to initiate at a shear force V_s.

FEMA 356 [15], Park [16], and Priestley [17] proposed estimating Δy using the secant stiffness at 0.6 Vy [Figure 2(a)], the secant stiffness at $0.75Vy$ [Figure 2(b)], and the initial tangent stiffness [Figure 2(c)], respectively. Mahin [18] estimated Δy using an equal area approach, as shown in Figure 2(d). In this paper, the method proposed by Park [16] is adopted.

The displacement ductility capacity of concrete walls depends on a wide range of factors, including axial load ratio, reinforcement ratio, geometry, and characteristics of the ground motion. Several methods have been used to provide an estimate for Δmax including assuming that it is equal to displacement at peak strength or displacement corresponding to 20% to 50% degradation from peak strength. For systems that involve severe strength and stiffness deterioration, the definition of maximum displacement to correspond to 20% to 50% degradation from peak strength may be incorrect [20]. In this research, Δmax is conservatively assumed to correspond to the peak load, which is defined in section 3 to correspond to failure of the steel bars, SMA bars, or concrete. Other failure modes, including buckling of steel bars and out-of-plane instability, were excluded, as the examined walls were assumed to be designed according to current seismic standards.

Salonikios et al. [22] found that V_s of steel RC walls correspond to about 75% to 80% of the ultimate strength. FEMA P698 [23] recommended using the same definition. In this paper, V_s is assumed to correspond to 75% of the ultimate wall strength, which was also experimentally observed for SMA RC walls by Abdulridha [4].

The ductility μ is defined as $\frac{\Delta max}{\Delta y}$. The same definition was used by NEHRP [19] and Uang [20]. The structure overstrength Ω results from design approximations, material overstrength, and redundancies in the lateral load system [16]. To account for the redundancies in the lateral load system, Ω can be defined as the ratio of peak lateral strength V_y to the shear force V_s corresponding to the first yielding displacement [20, 21]. Future probabilistic studies are needed to account for redundancies resulting from design approximations and material properties.

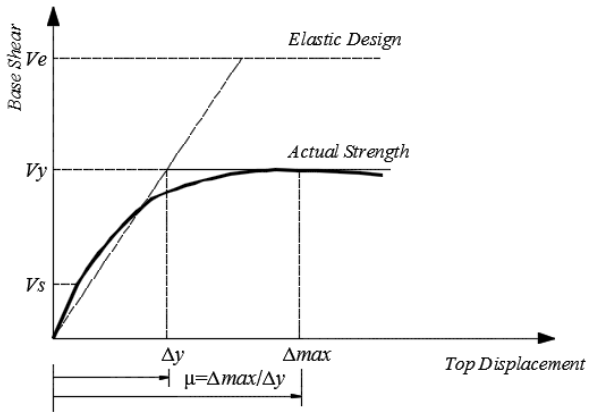

Figure 1. Relationship between base shear and top displacement

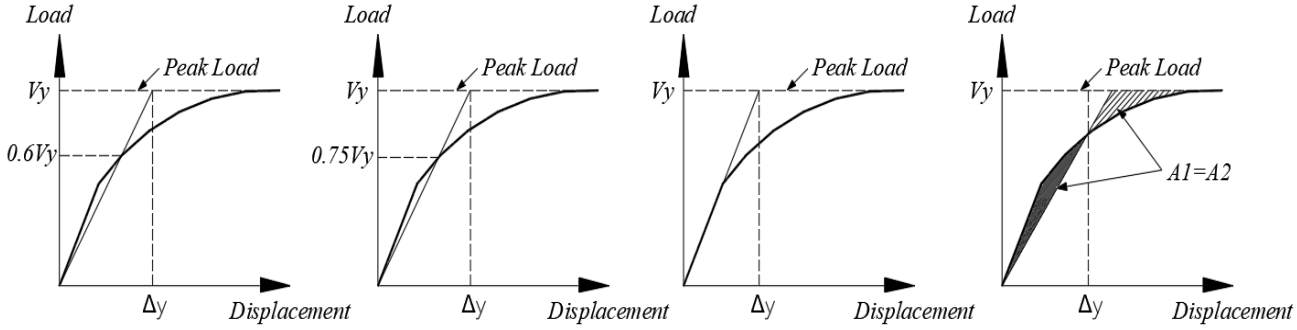

Figure 2. Definitions of yield displacement

Factors μ and Ω are used to calculate the force reduction factor R, which is equal to ΩR_μ. Factor R_μ can be calculated using Eq. 1, which was proposed by Newmark and Hall [24].

$$R_\mu = \begin{cases} \mu & \text{for } T_1 \geq 0.5 \text{ sec} \\ \sqrt{2\mu - 1} & \text{for } T_1 < 0.5 \text{ sec} \end{cases} \quad (1)$$

where T_1 is the fundamental structural period, determined using the effective stiffness K_{eff} [25], defined using Eq. (2),

$$K_{eff} = \alpha_v K_V \quad (2)$$

$$K_V = \frac{G b_w d}{f. h_w} \quad (3)$$

where α_v is axial load reduction factor, K_V is the secant shear stiffness at the first yield displacement [25], G is the shear modulus, b_w is the wall thickness, d is the effective wall length, f equals 1.2 for rectangular RC walls, and h_w is the wall height.

The following sections provide details about the model for SMA RC walls, the conducted numerical study to assess the values for Ω and R, and their evaluation using FEMA P695 [23].

3. Numerical Modeling

To predict the nonlinear response of SMA RC walls under reversed cyclic loading, the Shear-Flexural-Interaction Multi-Vertical-Line-Element (SFI-MVLE), developed and validated by Kolozvari [26] in the Open System Earthquake simulation software (OpenSees) [27], was utilized. The element accounts for interaction between the axial, flexural, and shear behaviour of moderate and slender RC shear walls [26]. The element and material constitutive relationships are shown in Figures 3 and 4, respectively. Figure 3 shows the use of three SFI-MVLEs to model a RC wall. Each element has six degrees of freedom, which capture the horizontal deformation, vertical deformation, and rotation at the center of the top and bottom rigid beams. Two-dimensional membrane RC panels are utilized to capture the flexural and shear behaviour of RC walls. Each panel accounts for the shear resistance using a fixed angle approach [26].

The flexural response is captured through the axial deformation u_y of the RC panels in the vertical direction. The average normal vertical strain $\varepsilon_{y,j}$ can be determined by dividing the average vertical deformation u_y by the element height h. The relative rotation between the top and bottom faces of the wall element is assumed to happen at a height Ch, measured from the bottom. The value of height coefficient C is recommended to be taken as 0.4 [26,28]. This rotation allows calculating the shear response (shear deformation u_{sh}) of the SFI-MVLE. The effect of increasing or decreasing the

number of RC panels or the number of SFI-MVLEs on the load-displacement curve of RC walls was found to be insignificant [26].

Figures 4a and 4b show the simplified Menegotto-Pinto hysteretic stress-strain model for the steel bars [29] and the biaxial concrete stress-strain model by Chang and Mander [30], respectively. Nickel-Titanium alloy (55.9% Nickel and 44.1% Titanium) is the most common type of superelastic SMA. Figure 4c describes the flag-shape of the NiTi SMA material model proposed by Christopoulos et al. [31]. The SMA stress f_{y-SMA} marks the phase transformation from austenite to martensite, and the change in stiffness from K_1 to K_2. Upon unloading from any strain less than a recoverable strain ε_r, the slope of the unloading path is K_1 until reaching βf_{y-SMA}, then it becomes K_2 until meeting the initial loading branch.

A strain limit of 5% was chosen as a conservative definition for failure of longitudinal steel bars under cyclic loading [32, 33, 34, 35, 36]. This conservative limit accounts for reduction in steel strains due to the nature of cyclic loading. For SMA bars, the recoverable strain ε_r is assumed 7%, which is the limit for the superelastic range [37]. The confined concrete compressive strain limit is assumed 2% [36].

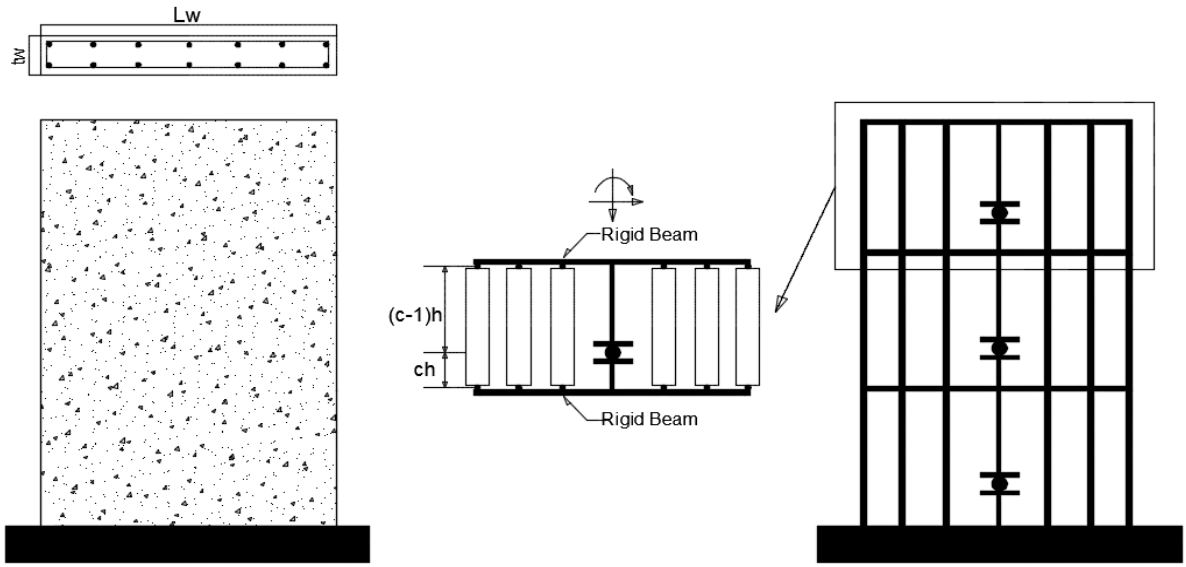

(a) (b)

Figure 3. RC wall model: (a) RC wall; (b) SFI-MVLE model

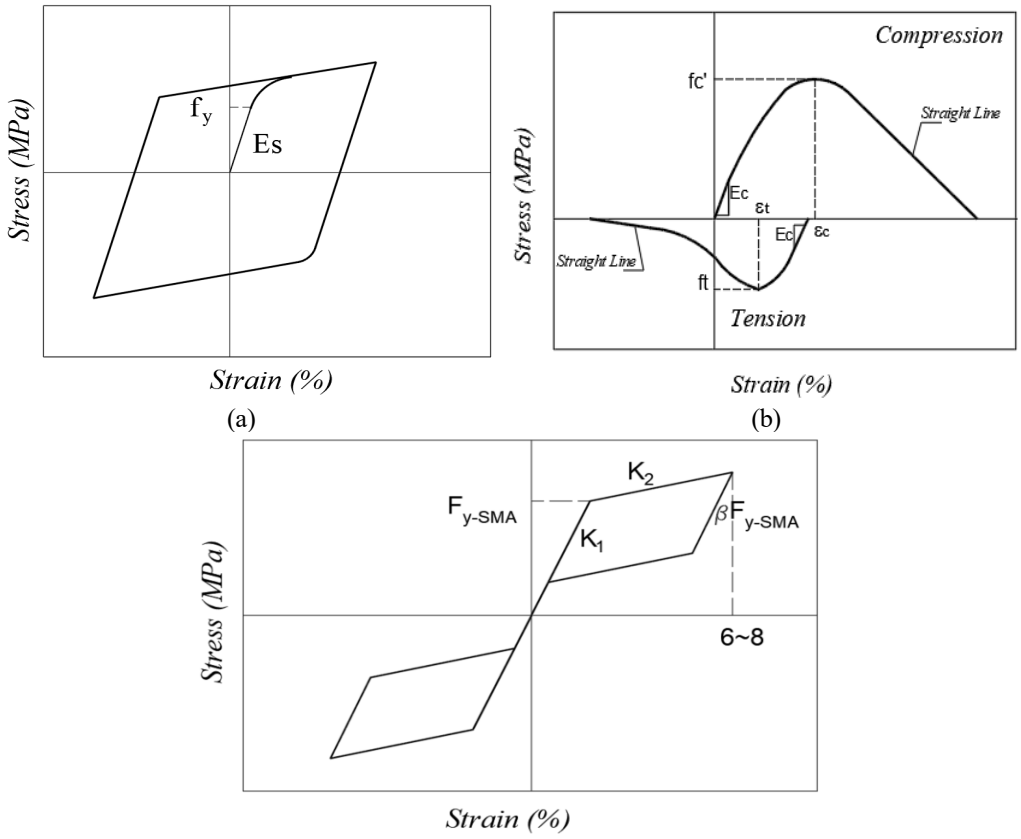

(a) (b)

(c)

Figure 4. Material constitutive relationships: (a) steel; (b) concrete; (c) SMA

In addition to the extensive validation conducted by Kolozvari [26] for the SFI-MVLE, additional validation cases were considered to ascertain its capabilities. An intermediate SMA RC wall, with an aspect ratio of 2.2, was experimentally tested by Abdulridha [4]. The SMA bars were located at the wall boundaries for the plastic hinge length, which was calculated based on CSA A23.3 [16]. The longitudinal reinforcement ratios in the wall boundaries and the wall web were 1.33% and 0.88%, respectively. The transverse reinforcement ratio was 0.88%. The values of f'_c, f_y, and f_{y-SMA} were 31, 425, and 380 MPa, respectively. The wall was modelled using two SFI-MVLE elements, one for the plastic hinge height and the second for the remaining height. Experimental and numerical results are shown in Figure 5. The SFI-MVLE model has accurately captured the peak shear strength (error of -5.7%), ultimate displacement (error of +5.5%), and residual displacement (error of -1.0%). It should be noted that modeling of the degradation in strength was not the focus for this research, as it does not affect the seismic design parameters, as defined in section 2. The cyclic response, shown in Figure 5, was terminated because of the rupture of steel bars, which were located on the wall web. This failure mode is identical to the experimental one, which was observed by Abdulridha (2012). The assumed identical behaviour of SMA bars in tension and compression is slightly different from the experiment, which can explain the discrepancy between the level of accuracy in predicting the tension and compression behaviour.

Kian and Cruz-Noguez [14] performed a test on an SMA RC wall with an aspect ratio of 2.2. The reinforcement ratios in the transverse and longitudinal directions were 0.4%. The reinforcement ratios for longitudinal bars of the boundary elements, longitudinal bars of the vertical web, and horizontal bars were 1.8%, 0.4%, and 1.0%, respectively. The values of f'_c, f_y, and f_{y-SMA} were 51, 421, and 330 MPa, respectively. The wall was modelled using two SFI-MVLE elements, one for the plastic hinge height and the second for the remaining height. The failure mode was associated with rupture

of the steel bars located in the web of the wall [14]. Figure 6 compares the experimental and numerical results. It illustrates that the numerical model has accurately captured the peak strength (error of +7%), peak displacement (error of +3), and ductility (error of -2.6%).

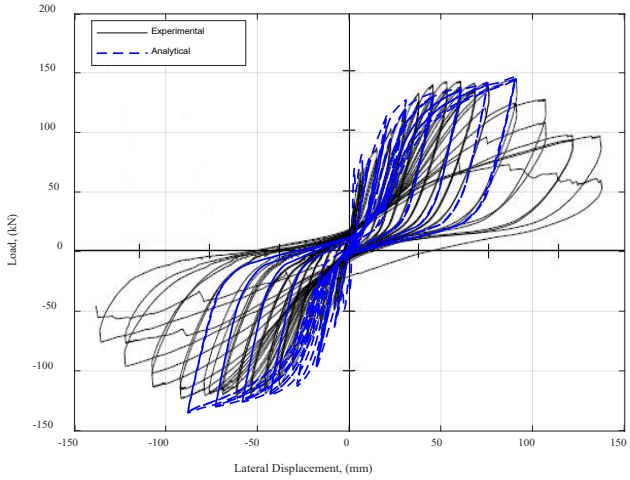

Figure 5. Comparison of experimental and numerical results for a SMA RC wall [4]

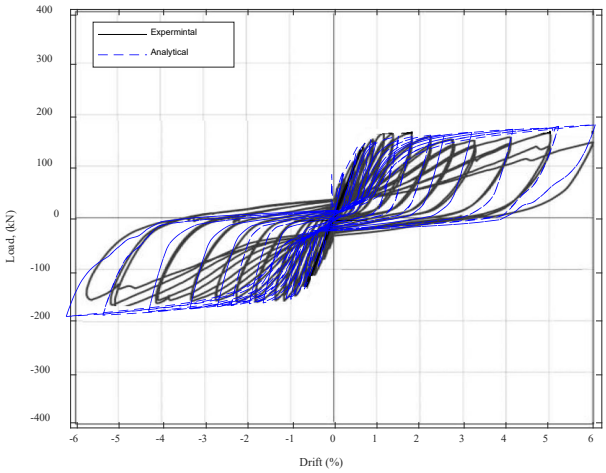

Figure 6. Comparison of experimental and numerical results for a SMA RC wall [14]

An experimental shake table test of an eight-story steel RC wall by Ghorbanirenani et al. [38] is used to investigate the sensitivity of the model discretization. Figure 7(a) shows the effect of the number of SFI-MVLEs per story. For the case of one SFI-MVLE per story, the variation of the height coefficient C is investigated in Figure 7(b). The results indicate that the effects of the number of vertical elements and the value of coefficient C are minor on the overall response. The numerical

model capability to capture the local wall response, considering the case of one element per story and C of 0.4, is illustrated in Figure 7(c) by showing the strain history for an outer bar. The model was able to predict the maximum strain values with reasonable accuracy. It should be noted that while the experimental results are based on strain gauge readings, the numerical results report the average strain over the wall height, which can describe the discrepancies in the results.

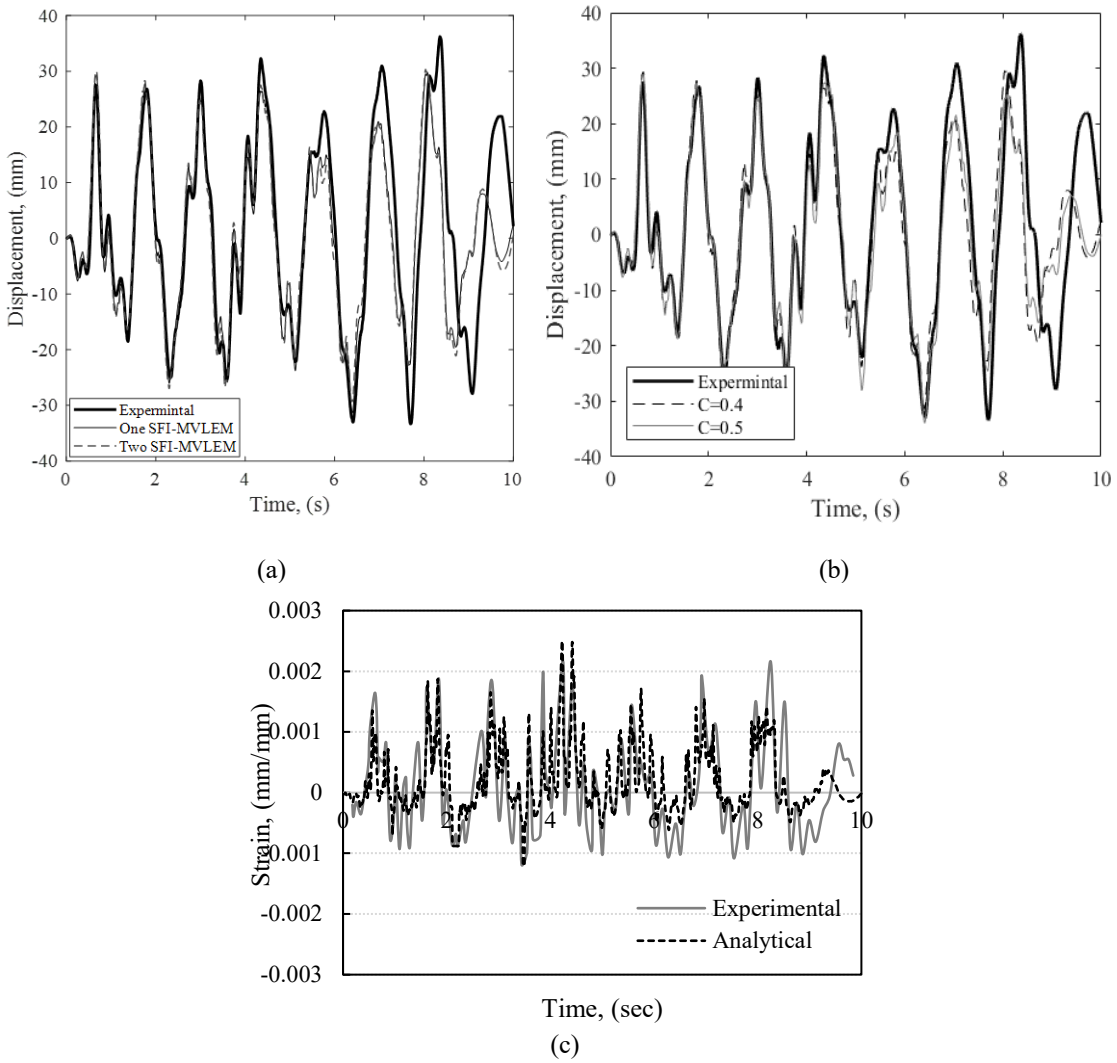

Figure 7. Comparison of experimental and numerical results for an SMA RC wall: (a) effect of the number of elements per story; (b) effect of C value; (c) strain history of an outer longitudinal steel bar

4. Evaluation of the Seismic Design Parameters

Nine-hundred and seventy-two SMA RC shear walls were analyzed. They cover the design parameters listed in Table 1. Axial load ratios were chosen within the range of $0 \leq P/(A_g f'_c) \leq 0.15$, as recommended by Priestley at al. [35]. Three typical wall thicknesses were chosen. The minimum transverse, web, and boundary reinforcement ratios (RFT) were taken as per CSA A23.3 [39]. Three boundary reinforcement ratios were selected, which are based on the minimum code requirement [39], recommendations by Wood [40] and by Bonelli et al. [41]. The steel bars were assumed to be replaced with SMA bars over the plastic hinge height, either for the full length of the wall (SMAPH), or only for the boundary elements (SMABW), as shown in Figures 8(a) and 8(b), respectively. Mechanical couplers were assumed to connect the SMA bars, used over the plastic hinge height, and the steel bars, used over the remaining height of the wall. The SMA bars were assumed to be rigidly connected to the steel bars, i.e., no slippage. This assumption is based on the experimental study conducted by Youssef et al. [2]. The smooth surface of the SMA bars was not modeled, because of their relatively small length and the fact that the mechanical couplers act as end anchors for them.

Figure 8(c) shows the two SFI-MVLEs utilized to model the plastic hinge zone and the remaining wall height. The wall was fixed at its base. A typical wall cross-section is shown in Figure 8(d). The axial load was first applied, and, then a reversed cyclic displacement-controlled loading protocol, Figure 8(e), was applied horizontally at the top of the wall. The loading protocol is based on the guidelines for cyclic seismic testing of components of steel structures [42] and was previously utilized by Abdulridha [4] to experimentally test SMA RC walls.

The parametric study revealed that the displacement ductility μ and overstrength factor are influenced by the amount of boundary reinforcement and axial load. The influence of the remaining parameters (wall aspect ratio, wall thickness, and horizontal steel ratio) was found to be minimal. The ductility

was reduced by 37% on average, when the boundary reinforcement ratio increased from 0.5% to 1.5%. This reduction is due to the low modulus of elasticity of the SMA bars, which resulted in large yield displacements. On the other hand, increasing the axial load increased the ductility as it increased the flexural capacity and associated deformations. The overstrength factor increased by 26% on average with increasing the boundary element reinforcement ratio from 0.5% to 1.5%. Increasing the axial load ratio from 2% to 10% slightly reduced the overstrength factor due to the increase in Vs value. SMAPH walls experienced greater displacement recovery than SMABW walls. Considering aspect ratios from 1.5 to 6.0 and wall thicknesses from 150 mm to 230 mm, the average displacement recovery is 96% for SMAPH walls and 73% for SMABW walls.

The response modification factor R and overstrength factor Ω were determined for the mentioned 972 walls. Figure 9 shows a whisker chart, giving the mean, maximum, minimum, 25%, and 75% of the estimated R and Ω values for both SMAPH and SMABW walls based on their aspect ratio and SMA locations. The mean R values are 2.5 and 3.0 for SMAPH walls with aspect ratio <2.0 and >2.0, respectively, whereas the mean R values for SMABW walls with aspect ratio <2.0 and >2.0 are 3.0 and 4.0, respectively. The corresponding coefficient of variations (COV) are 20% and 16% for SMAPH walls with aspect ratio <2.0 and >2.0, respectively; and 20% and 19% for SMABW walls with aspect ratio <2.0 and >2.0, respectively. The mean value of Ω is 2.25 for SMAPH and SMABW walls. The corresponding COVs are 21% for SMAPH walls and 18% for SMABW walls. The almost constant ratio for the overstrength factor indicates a consistent level of safety for the considered walls.

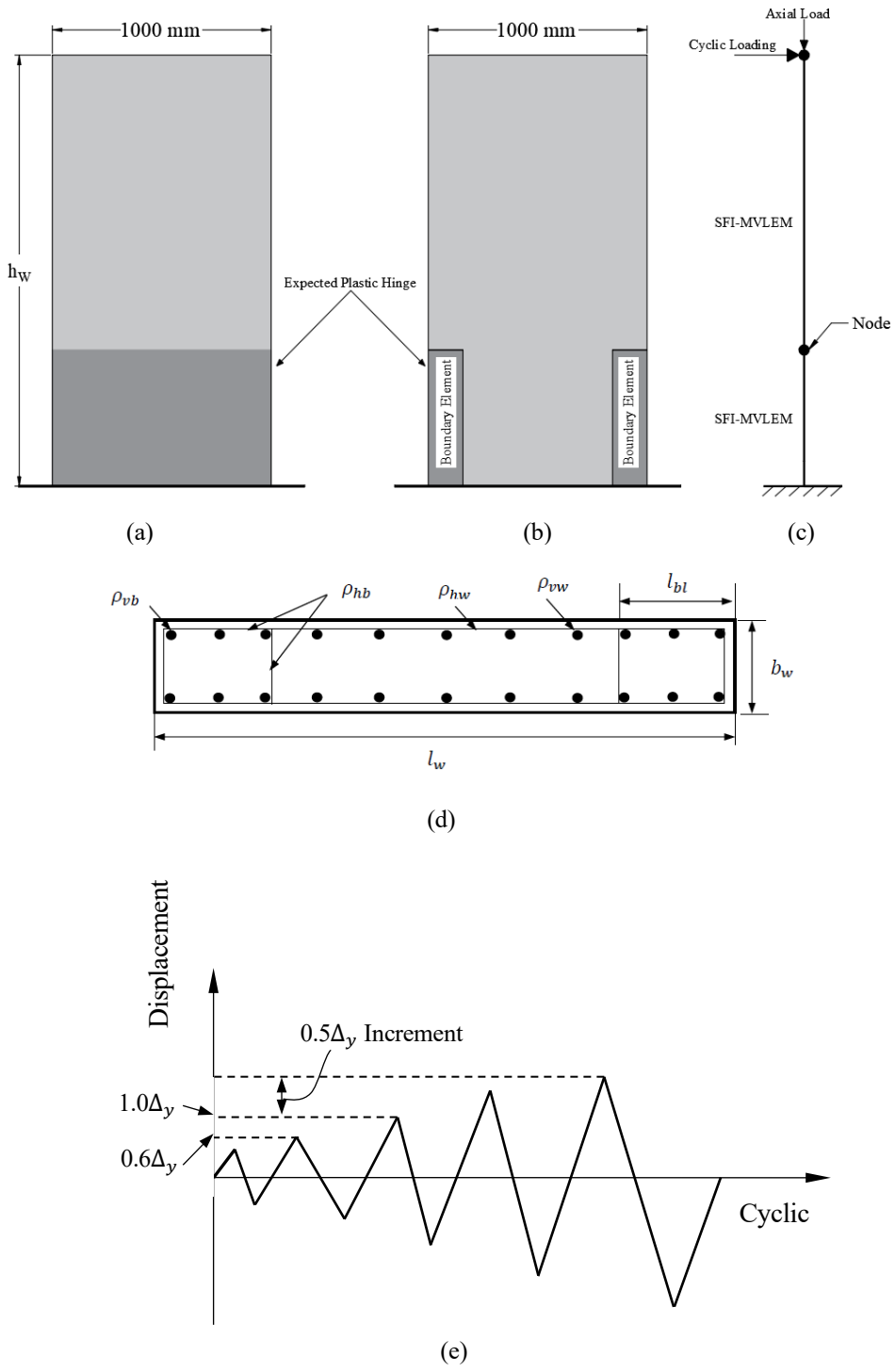

Figure 8. Numerical study details (a) SMAPH RC wall; (b) SMABW RC wall; (c) SFI-MVLE Model; (d) typical wall section; (e) cyclic loading

Table 1. Range of parameters selected for the considered walls

	Aspect Ratio (AR)	Period (sec)	Wall Thickness (b_w) (mm)	Axial Load Ratio [1] %	Transverse RFT (ρ_{hw}) %	Web RFT (ρ_{vw}) %	Boundary RFT (ρ_{vb}) %
Case 1	6.0	>0.5	150, 200, 230	2, 7.5, and 10	0.25, 0.5, and 1	0.5, 0.66, 0.75, and 1	0.5, 1.0, and 1.5
Case 2	3.0	<0.5	150, 200, 230	2, 7.5, and 10	0.25, 0.5, and 1	0.5, 0.66, 0.75, and 1	0.5, 1.0, and 1.5
Case 3	1.5	<0.5	150, 200, 230	2, 7.5, and 10	0.25, 0.5, and 1	0.5, 0.66, 0.75, and 1	0.5, 1.0, and 1.5

[1] Axial Load Ratio = $\frac{P}{A_g f'_c}$

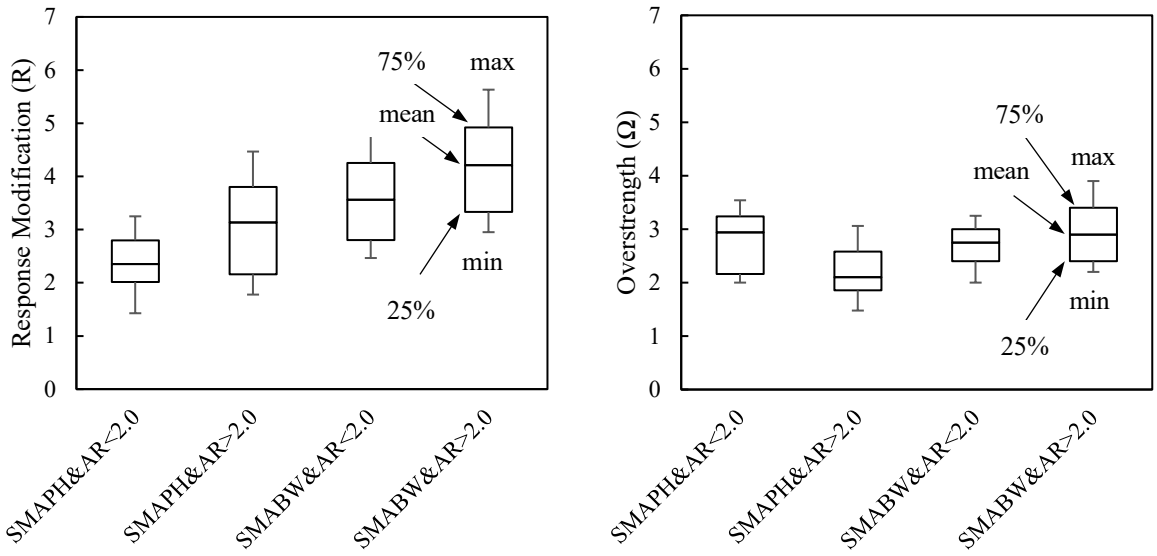

(a) (b)

Figure 9. Seismic Design Parameters:(a) R factor; (b) Ω factor

5. Assessment of the Evaluated Seismic Design Parameters

Three buildings, located in Vancouver, BC, were designed using RC ductile walls to resist lateral loads in the short direction, as shown in Figure 10. The three buildings had different heights (3, 6, and 9 stories) with a typical story height of 3 m. The walls were designed using the equivalent lateral load procedure of the current Canadian standards, CSA A23.3 [39] and NBCC [43]. As the Canadian standards do not have values for the overstrength and ductility factors for SMA RC walls, the mean values obtained in the previous section were utilized. The concrete compressive strength and steel yield strength were assumed to be 30 MPa and 400 MPa, respectively. The length of the walls was first assumed, and then an acceptable thickness and area of the vertical steel were evaluated. The horizontal steel ratio satisfied the minimum requirement by the standard [39].

The steel bars were then assumed to be replaced by SMA bars over the plastic hinge length (L_p), given by Eq. 4 of CSA A23.3 [39]. The SMA bars were utilized for the full wall length of SMAPH

walls, and only in the boundary elements of SMABW walls. Details of the designed walls are given in Table 2.

$$L_p = 0.5l_w + 0.1h_w \quad (4)$$

where l_w is the wall length and h_w is the wall height

Each wall was modeled using one SFI-MVLE per story except for the first story, which was modeled using two elements to represent the plastic hinge height and the remaining story height. Eigenvalue analysis is performed using OpenSees [27] to obtain the first period T_1 for each building. The designed walls were then analyzed using incremental dynamic analysis (IDA) [44] to evaluate their seismic performance. For each building, twenty earthquake ground motions were selected from the PEER Next Generation Attenuation database [45] The chosen records represent spectra period range from $0.2T_1$ to $1.5T_1$. The site class was conservatively assumed to be D, with shear wave velocity ranging from 180 m/s to 360 m/s. The ground motion was scaled to match the site design spectra acceleration of Vancouver, BC. Figure 11 shows the mean elastic response spectra of these ground motions assuming 5% damping. The analysis was stopped when any of the local failure criteria is observed.

The validity of the used seismic design parameters was assessed using the methodology recommended by FEMA P695 [23], which quantifies response parameters for use in seismic design. This methodology provides a rational basis for evaluating the global seismic performance factors, including the response modification coefficient (R) and the system overstrength factor (Ω) of new seismic-force-resisting systems to allow inclusion in building codes. The evaluation process assures that the new system will result in equivalent safety against a collapse in an earthquake, comparable to the inherent safety against collapse intended for known seismic-force-resisting systems.

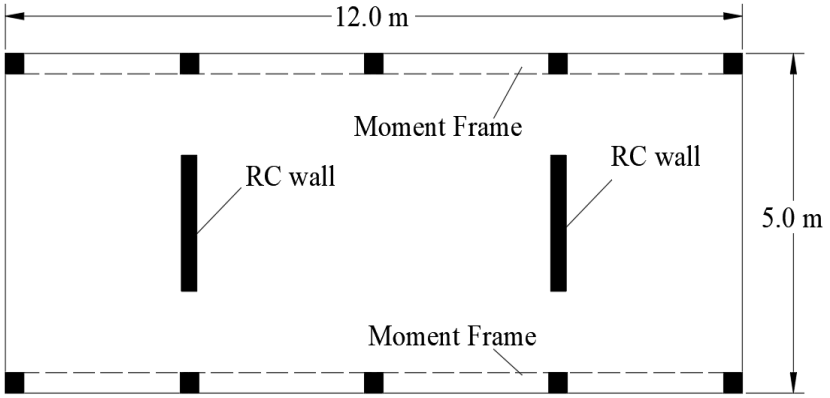

Figure 10. Considered structural plan

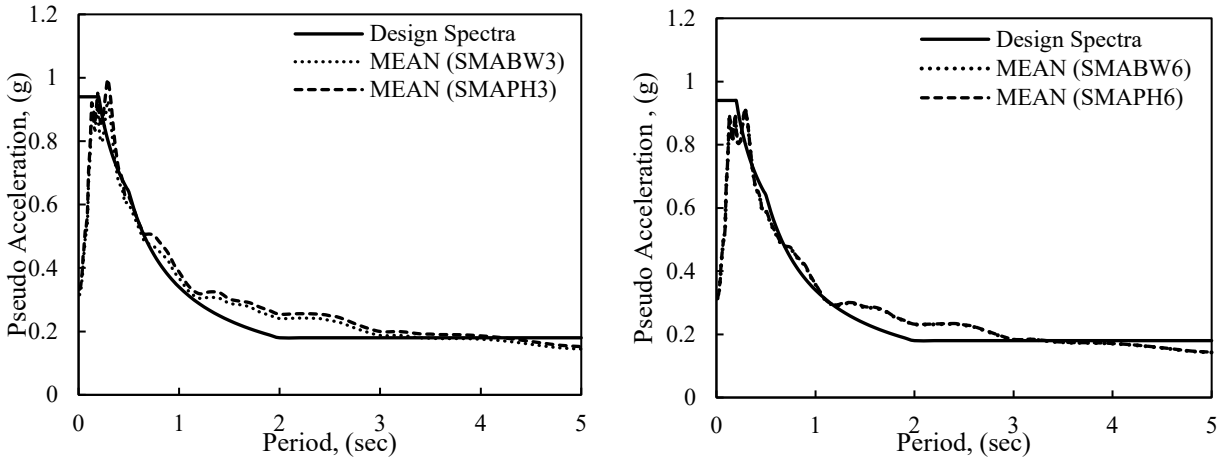

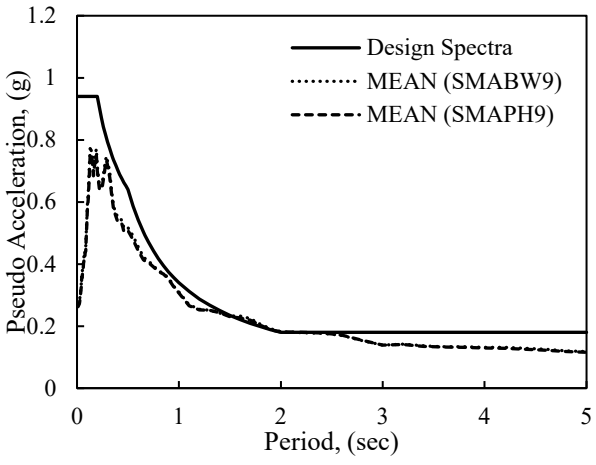

(c)

Figure 11. Design and pseudo acceleration: (a) three-story walls; (b) six-story walls; and (c) nine-story walls

Table 2. Walls design details.

	3-story		6-story		9-story	
	SMAPH	SMABW	SMAPH	SMABW	SMAPH	SMABW
T_1(sec)	0.61	0.69	1.13	1.15	1.90	2.10
Wall thickness (b_w)	250 mm	200 mm	250 mm		300 mm	250 mm
Wall length (l_w)	1200 mm		1800 mm		2000 mm	
Boundary element length (l_{bl})	300 mm		300 mm		400 mm	
Horizontal steel ratio (web) (ρ_{hb})	0.25%		0.25%		0.25%	
Horizontal steel ratio (boundary)	0.25%		0.25%		0.25%	
Vertical RFT ratio (web) (ρ_{VW})	0.8%	1.0%	1.33%		1.11%	1.33%
Vertical RFT ratio (boundary) (ρ_{Vb})	2.4%	3.0%	2.4%		2%	2.4%

Collapse fragility curves, showing the intensity measure of the ground motion versus the probability of collapse, were developed using the fitting method [46] and are shown in Figure 12. The 5% damped spectral acceleration at the first period [Sa (T1, 5%)] defines the used intensity measure. FEMA P695 [23] defines the collapse probability at 50% as the median collapse intensity ($\hat{S}_{CT}$), as shown in Figure 12. The collapse margin ratio (CMR) can be calculated as the ratio of $\hat{S}_{CT}$ to the spectral acceleration of the maximum considered earthquake corresponding to the fundamental period (S_{MT}) assuming 5% damping ratio, Eqs. 5 through 7.

$$CMR = \frac{\hat{S}_{CT}}{S_{MT}} \tag{5}$$

$$S_{MT} = S_{MS} \quad \text{for} \quad T_1 < T_s \tag{6}$$

$$S_{MT} = \frac{S_{M1}}{T_1} \quad \text{for} \quad T_1 > T_s \tag{7}$$

where S_{MS} and $S_{M1}$are the modified spectral values at the fundamental period and at one second considering the maximum design earthquake, respectively.

The CMR ratio was then modified to account for the modal uncertainty (β_{TOT}) and spectral shape factor (SSF). The modification is based on the structure fundamental period and the period-based ductility, $\mu_T = \delta_u/\delta_{y,eff}$. Values of β_{TOT} and SSF can be determined from Tables 9-4 and 9-5 in FEMA P695 [23]. The μ_T is evaluated considering three options: (1) maximum base shear and maximum displacement (Max Disp-Max V), (2) maximum displacement and the corresponding base shear (Max Disp-V), and (3) maximum base shear and the corresponding displacement (Max V-Disp.). Figure 13 shows the evaluated mean IDA displacement versus shear, considering the three options. The corresponding values of μ_T are summarized in Table 3. The lowest μ_T was then utilized, as it provides a lower SFF value, which leads to a conservative design. In all cases, the maximum base shear, and the corresponding displacement (Max V-Disp) approach led to about 80% of the

lowest μ_T values. A modified collapse margin ratio (ACMR) for each wall was then calculated using Eq. 8. The calculated ACMR values were compared to the individual ACMR $_{limit}$ provided by FEMA P695 [23].

$$ACMR = SFF \times CMR \quad (8)$$

The average ACMR for SMAPH and SMABW walls were compared to the minimum acceptable ACMR values provided by FEMA P695 [23]. Table 4 summarizes the calculations for ACMR and the FEMA P695 [23] acceptance criteria. The designed walls met the individual and the average acceptance criteria and provided an acceptable seismic performance, which reflects the adequacy of the used seismic design parameters. The collapse margin ratio was found to increase with the building height, reflecting that the seismic design parameters can be made dependent on the building height.

Table 3. Period-based ductility

Building ID	Period-based ductility (μ_T)			
	Max Disp-Max V	Max Disp-V	Max V- Disp.	Used
3-SMABW	2.7	2.8	1.8	1.8
3-SMAPH	3.5	3.6	1.7	1.7
6-SMABW	2.7	3.0	2.7	2.7
6-SMAPH	2.1	2.8	1.6	1.6
9-SMABW	2.4	2.2	3.3	2.2
9-SMAPH	2.5	4.3	2.5	2.5

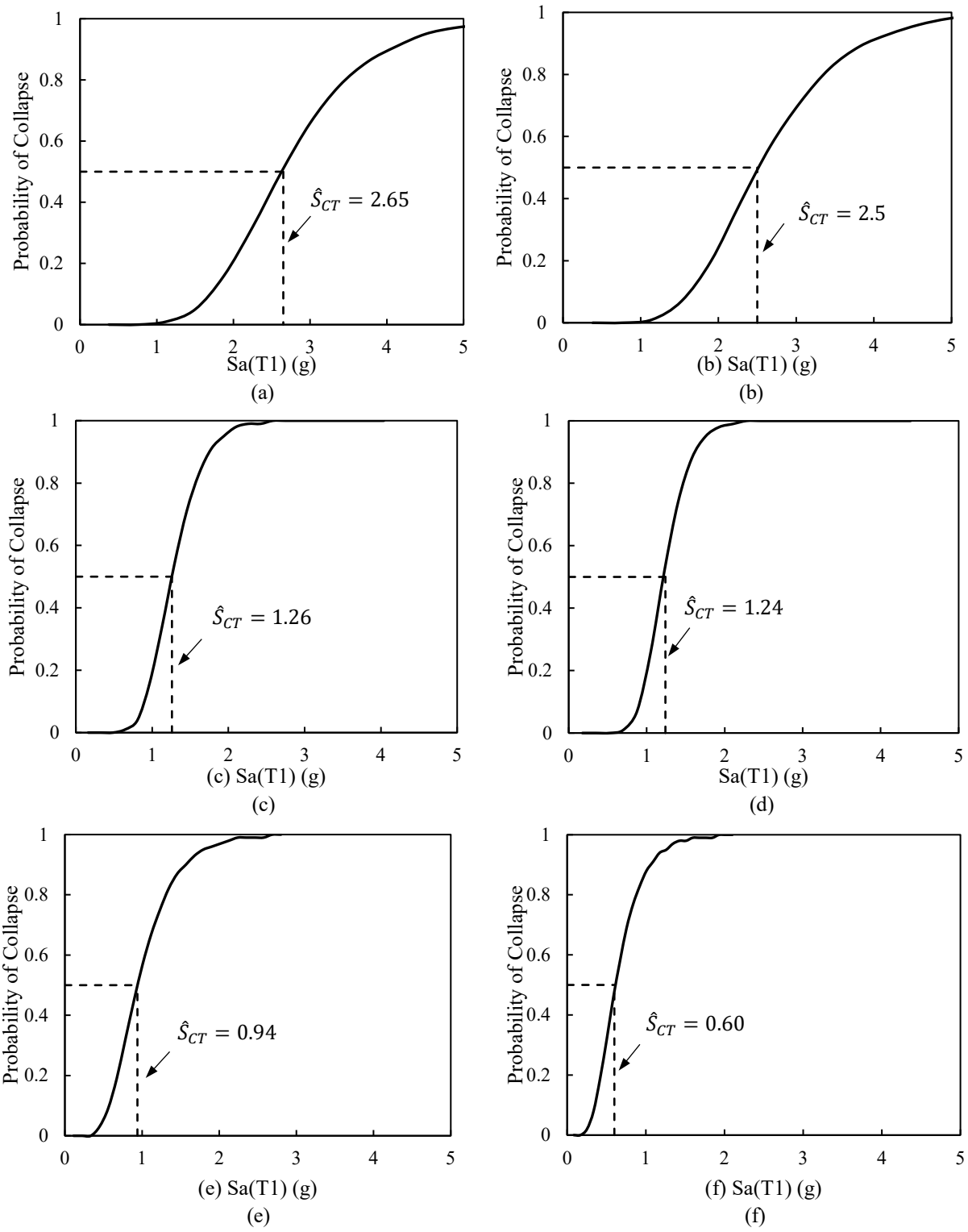

Figure 12. Fragility curves:

(a) 3-SMAPH; (b) 3-SMABW; (c) 6-SMAPH; (d) 6-SMABW; (e) 9-SMAPH; (f) 9-SMABW

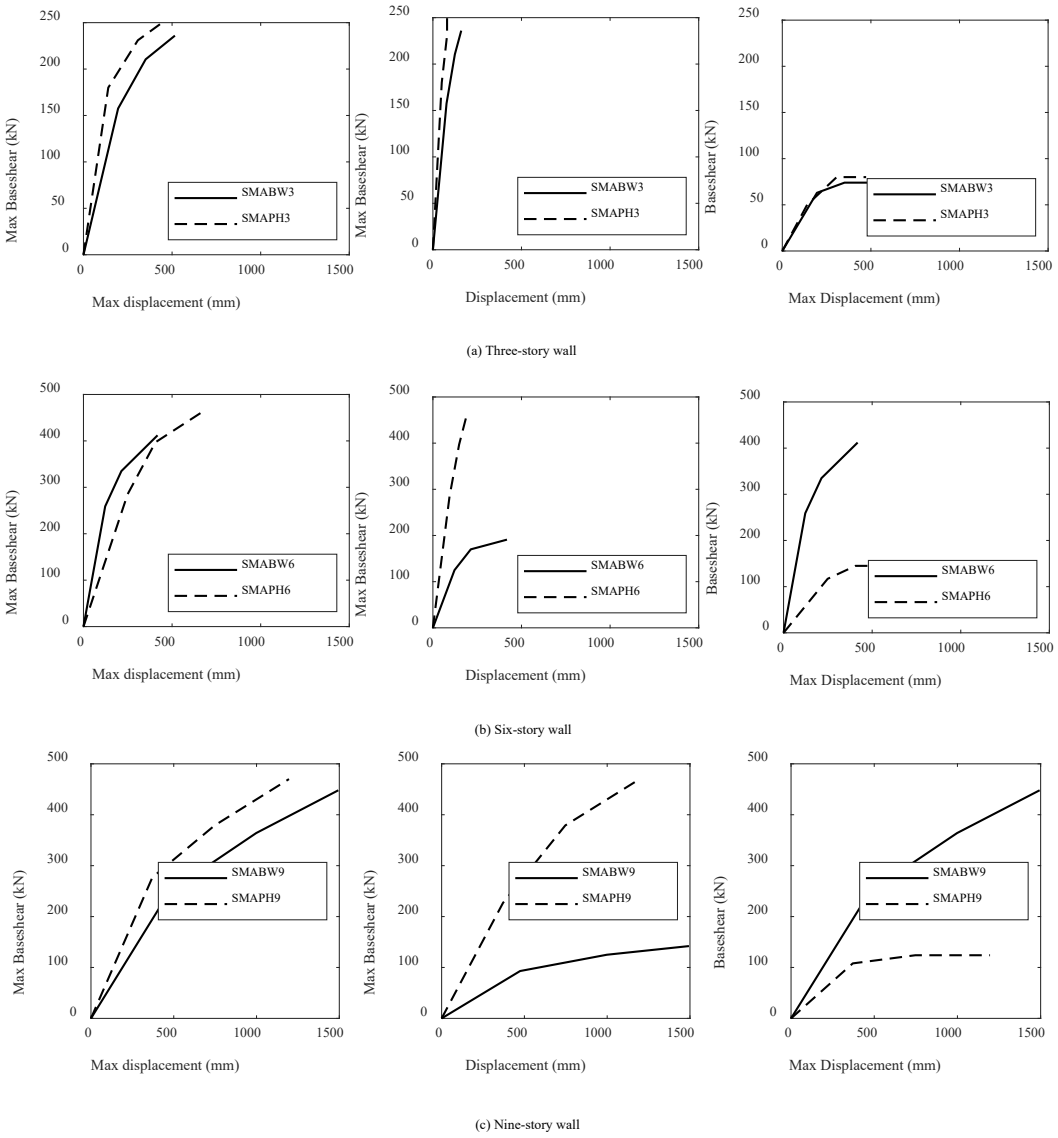

Figure 13. Pushover curve obtained from IDA: (a) three-story, (b) six-story, and (c) nine-story

Table 4. Seismic design parameters assessment by FEMA P695 [23]

Building Group	Building ID	Height (m)	$\hat{S}_{CT}$	CMR	μ_t	SFF	ACMR	β_{TOT}	$ACMR_{minimum}$ FEMA P-695	Pass/Fail
1	SMAPH	9	2.65	3.00	1.70	1.11	3.30	0.50	1.52	Pass
		18	1.26	4.07	1.60	1.15	4.68	0.50		
		36	0.94	4.73	2.50	1.19	5.63	0.50		
		Mean		3.93	1.93	1.22	4.80	0.50	1.90	
2	SMABW	9	2.50	2.77	1.80	1.12	3.10	0.50	1.52	Pass
		18	1.24	3.74	2.70	1.24	4.64	0.50		
		36	0.60	6.67	2.20	1.23	8.20	0.50		
		Mean		4.40	2.23	1.22	5.37	0.50	1.90	

6. Conclusions

In this paper, the response modification factor (R) and the Overstrength factor (Ω) for SMA RC walls were assessed through a numerical study. The SMA bars were only used in the plastic hinge zone. Two potential arrangements were considered: SMA bars at the wall boundary elements (SMABW) and SMA bars replacing all web and boundary element steel bars (SMAPH). A total of 972 walls were analyzed to identify the effect of wall design parameters on seismic performance and to estimate the seismic design parameters. Three case study buildings were then designed using the obtained parameters. FEMA P695 [23] methodology was utilized to assess the adequacy of the obtained seismic design parameters. Conclusions from this study can be summarized in the following points.

1. The displacement ductility μ and overstrength factor are influenced by the amount of boundary reinforcement and axial load. The influence of the remaining parameters (wall aspect ratio, wall thickness, and horizontal steel ratio) was found to be minimal.
2. SMAPH walls experienced greater displacement recovery than SMABW walls.
3. For walls with $\frac{h_w}{l_w} < 2.0$, values of the obtained response modification factor R are 2.5 and 3.5 for SMAPH and SMABW walls, respectively. For walls with $\frac{h_w}{l_w} > 2.0$, values of the obtained R are 3.0 and 4.0 for SMABW and SMABW walls, respectively. The obtained overstrength factor is 2.25 for both SMAPH and SMABW walls.
4. Utilizing SMA bars in the RC wall designed, using the current design standards and the obtained seismic design parameters, has resulted in an acceptable seismic performance based on FEMA-P695 criteria.
5. The variation in the collapse margin ratio with the building height indicates the need for making the seismic design parameters function of the building height.

6. The obtained seismic design parameters are based on simplified models, which require further studies to reach reliable values. In this study, the ductility is conservatively assumed to be corresponding to the peak strength. Future studies, which provide better evaluation for the ductility based on experimental results, are needed. Future probabilistic studies are also needed to account for redundancies resulting from design approximations and material properties on the overstrength factor. The use of the seismic design parameters for other structural configurations needs also to be assessed.

Acknowledgment
The authors are grateful for the financial support provided by the Natural Sciences and Engineering Research Council of Canada (NSERC).

7. References

[1] Youssef M, Elfeki M. Seismic performance of concrete frames reinforced with superelastic shape memory alloys. Smart Structures and Systems 2012; 9(4): 313-333.

[2] Youssef M, Alam M, Nehdi M. Experimental investigation on the seismic behaviour of beam-column joints reinforced with superelastic shape memory alloys. Journal of Earthquake Engineering 2008; 12(7): 1205-1222.

[3] Alam M, Youssef M, Nehdi M. Analytical prediction of the seismic behaviour of superelastic shape memory alloy reinforced concrete elements. Engineering Structures 2008; 30(12): 3399-3411.

[4] Abdulridha A. Performance of superelastic shape memory alloy reinforced concrete elements subjected to monotonic and cyclic loading. Ottawa: Ph.D. thesis 2012: University of Ottawa.

[5] Tazarv M, Saiidi M. Analytical studies of the seismic performance of a full-scale SMA-reinforced bridge column. International Journal of Bridge Engineering 2013; 1(1): 37-50.

[6] Effendy E, Liao W, Song G, Mo Y, Loh C. Seismic behavior of low rise shear walls with SMA bars. Earth & Space 2006; 3: 377-388.

[7] Ghassemieh M, Mostafazadeh M, Sadeh M. Seismic control of concrete shear wall using shape memory alloys. Journal of Intelligent Material Systems and Structures 2012; 23(5): 535-543.

[8] Abraik E, Youssef M. Cyclic performance of shape memory alloy reinforced concrete walls. Response of structures under extreme loading (pp. 326-333). Lansing, MI 2015: The fifth international workshop on performance, protection, and strength of structures under extreme loading.

[9] Abraik E, Youssef M. Performance assessment of three-story shape memory alloy reinforced concrete walls. CSCE 5th International Structural Specialty Conference 2016; 852. London, ON, Canada.

[10] Ghassemieh M, Rezapour M, Sadeghi V. Effectiveness of the shape memory alloy reinforcement in concrete coupled shear walls. Journal of Intelligent Material Systems and Structures 2017; 28(5): 640-652.

[11] Rezapour M, Ghassemieh M. Macroscopic modelling of coupled concrete shear wall. Engineering Structures 2018; 169: 37-54.

[12] Abraik E, Youssef M. Seismic fragility assessment of superelastic shape memory alloy reinforced concrete shear walls. Journal of building engineering 2018; 19: 142-153.

[13] Abraik E, Youssef M. Seismic performance of shape memory alloy reinforced concrete dual systems. 16TH European Conference on Earthquake Engineering 2018; Thessaloniki, Greece.

[14] Tolou Kian M J, Cruz-Noguez C. Reinforced Concrete Shear Walls Detailed with Innovative Materials: Seismic Performance. Journal of Composites for Construction 2018; 22(6): 04018052.

[15] FEMA356. (2000). Prestandard and Commentary for the seismic rehabilitation of buildings. Washington, DC: federal emergency management agency.

[16] Park R. Sate-of-the art report- ductility evaluation from laboratory and analytical testing. Proceedings of Ninth World Conference on Earthquake Engineering 1988; August 1988, Vol. VIII, pp. 605-616. Tokyo-Kyoto, Japan.

[17] Priestley M, Park R. Strength and ductility of concrete bridge columns under seismic loading. ACI Struct J 1987; 84(1): 61-76.

[18] Mahin S, Bertero V V. Problems in establishing and predicting ductility in structural design. Proceedings of international symposium on earthquake structural engineering 1976; 1: pp. 613-628. St. Louis, Mo.

[19] The national earthquake hazards reduction program (NEHRP) 2009: Dept. of the Interior, US Geological Survey.

[20] Uang C. Establishing R (or Rw) and Cd factors for building seismic provisions, ASCE. Journal of Structural Engineering 1991; 117(1).

[21] Annan C D, Youssef M A, El Naggar M H. Seismic overstrength in braced frames of modular steel buildings. Journal of Earthquake Engineering 2008; 13(1): 1-21.

[22] Salonikios T N, Kappos A J, Tegos I A, Penelis G G. Cyclic load behavior of low-slenderness reinforced concrete walls: failure modes, strength and deformation analysis, and design implications. ACI Structural Journal 2000; 97(1): 132-141.

[23] FEMA. (2009). Quantification of building seismic performance factors, federal emergency management agency. FEMA P695, Washington, DC.

[24] Newmark N M, Hall W J. Earthquake spectra and design. Engineering Monograph, Earthquake Engineering Research Institute 1982; Berkeley, USA.

[25] Park R, Paulay T. (1975). Reinforced concrete structures. John Wiley & Sons.

[26] Kolozvari K. Analytical modeling of cyclic shear-flexural interaction in reinforced concrete structural walls. Ph.D. 2013; Thesis, University of California, Los Angeles, USA.

[27] OpenSees. (2018). Open system for earthquake engineering simulation. Berkeley, CA.

[28] Orakcal K, Wallace J W, Conte J P. Nonlinear modeling and analysis of reinforced concrete structural walls. ACI Structural Journal 2004; 101(5): 688-698.

[29] Menegotto M, Pinto P. Method of analysis of cyclically loaded RC plane frames including changes in geometry and non-elastic behavior of elements under normal force and bending 1973; Preliminary Report ABSE, vol 13.

[30] Chang G, Mander J. Seismic energy based fatigue damage analysis of bridge columns: Part I-evaluation of seismic capacity 1994; Buffalo, New York: NCEER-94-0006. State University of New York.

[31] Christopoulos C, Tremblay R, Kim H.-J, Lacerte M. Self-centering energy dissipative bracing system for the seismic resistance of structures: development and validation. Journal of Structural Engineering ASCE 2008; 134(1): 96-107.

[32] Blume J A, Newmark N M, Corning L H. Design of multi-story reinforced concrete buildings for earthquake motions. Portland Cement Association 1961; Chicago, IL: 318 pp.

[33] Scott B D, Park R, Priestley M J. Stress-strain behaviour of concrete confined by overlapping hoops at low and high strain rates. ACI Journal Proceeding 1982; 79(1): 13-27.

[34] Paulay T, Priestley M. Seismic design of reinforced concrete and masonry buildings 1992; New York, NY, USA: John Wiley & Sons.

[35] Priestley M, Calvi G, Kowalsky M. Displacement based seismic design of structures 2007; IUSS Press: Pavia, Italy.

[36] Panagiotou M. Ph.D. thesis: Seismic design, testing, and analysis of reinforced concrete wall buildings 2008; UC: San Diego.

[37] Hurlebaus S, Gaul L. Smart structure dynamics. Mechanical system and signal 2006; 255-281.

[38] Ghorbanirenani I, Tremblay R, Léger P, Leclerc M. Shake table testing of slender RC shear walls subjected to eastern North America seismic ground motions. Journal of Structural Engineering 2012; 138(12): 1515-1529.

[39] A23.3-14. Design of Concrete Structures. Canadian Standards Association 2014; Mississauga, ON, Canada.

[40] Wood S L. Minimum tensile reinforcement requirements in walls. ACI Structural Journal 1989; Vol. 86: No. 5, pp. 582–591.

[41] Bonelli P, Tobar R, Leiva G. Experimental study on failure of reinforced concrete building. ACI Structural Journal 1999; Vol. 96, No. 1: pp. 3–8.

[42] ATC. Guidelines for Cyclic Seismic Testing of Components of Steel Structures 1992; American Iron and Steel Institute.

[43] NBCC. National Building Code of Canada. National research council of Canada 2015; Ottawa.

[44] Vamvatsikos D, Cornell C. Incremental dynamic analysis. Earthquake Engineering and Structural Dynamics 2001; 31(3): 491-514.

[45] PEER Ground Motion Database. (2018). Retrieved from https://ngawest2.berkeley.edu/

[46] Baker J W. Efficient analytical fragility function fitting using dynamic structural analysis. Earthquake Spectra 2015; 31(1): 579-599.

NOMENCLATURE

P	Axial load ratio
α_v	Axial load reduction factor
$ACMR$	Adjusted collapse margin ratio
$\varepsilon_{y,j}$	Average normal vertical strain
u_y	Average vertical deformation
A_g	Cross-section area
f'_c	Concrete compression strength
E_c	Concrete modulus of elasticity
ε_c	Concrete compression strain
ε_t	Concrete tensile strain
G	Concrete shear modulus
f_t	Concrete tensile strength
CMR	Collapse margin ration
R_μ	Ductility response factor
μ	Ductility factor
V_e	Elastic base shear
K_{eff}	Effective stiffness
d	Effective wall length
h	Element height
V_s	First yield strength
C	height coefficient

K_1	Initial stiffness
Δ_y	Lateral yielding displacement
Δ_{max}	Maximum displacement corresponding to peak shear strength
$\hat{S}_{CT}$	Median collapse capacity
S_{MT}	Maximum considered earthquake corresponding to the fundamental period
S_{MS}	Modified spectral values at the fundamental period
S_{M1}	Modified spectral values at one second
β_{TOT}	Modal uncertainty
Ω	Overstrength factor
μ_T	Period-based ductility
L_P	Plastic hinge length
K_2	Post-Activation Stiffness
R	Response modification factor
ε_r	Recoverable strain
K_V	Secant shear stiffness at the first yield displacement
SSF	Spectra shape factor
T_1	Structure fundamental period
SMA	Superelastic shape memory alloy
f_y	Steel yield strength
E_s	Steel modulus of elasticity
$S_a(T_1)$	Spectra acceleration at fundamental period
f_{y-SMA}	Shape memory alloy yield strength

u_{sh}	Shear deformation
V_y	Wall peak lateral strength
h_w	Wall height
l_w	Wall length
b_w	Wall thickness
l_{bl}	Wall boundary length
ρ_{vb}	Wall vertical boundary reinforcement ratio
ρ_{hb}	Wall horizontal boundary reinforcement ratio
ρ_{vw}	Wall vertical web reinforcement ratio
ρ_{hw}	Wall horizontal web reinforcement ratio